Synthesis, characterization, crystallographic structure, theoretical studies, and in vitro cytotoxicity assessment of two Gd(III) and Ce(IV) complexes containing pyridine-2,6-dicarboxylate

Synthesis, characterization, crystallographic structure, theoretical studies, and in vitro cytotoxicity assessment of two Gd(III), Ce(IV) complexes of pyridine-2,6-dicarboxylic acid

Mina Zohrevani[a], Sara Abdolmaleki[a], Mohammad Ghadermazi[*,a], Yasin Gholiee[*,b], Alireza Aliabadi[c], Elham Motieiyan[d], Mohammad Hakimi[d] and Domenica Marabello[e,f]

[a] *Department of Chemistry, Faculty of Science, University of Kurdistan, Sanandaj, Iran. E-mail: mghadermazi@yahoo.com, mghadermazi@uok.ac.ir*

[b] *Department of Chemistry, Faculty of Science, Malayer University, Malayer, Iran. E-mail: yasingholiee@gmail.com, yasingholiee@malayeru.ac.ir*

[c] *Pharmaceutical Sciences Research Center, Health Institute, School of Pharmacy, Kermanshah University of Medical Sciences, Kermanshah, Iran.*

[d] *Department of Chemistry, Payame Noor University, P. O. BOX 19395-4697, Tehran, Iran.*

[e] *Dipartimento di Chimica, University of Torino Via P. Giuria 7, 10125 Torino, Italy.*

[f] *Interdepartmental Centre for Crystallography, University of Torino, Italy*

Abstract

This paper reports the synthesis of two complexes through one-pot reactions of pyridine-2,6-dicarboxylic acid ($pydcH_2$), phenanthroline, and 2-aminopyridine, with $Gd(NO_3)_3.6H_2O$ and $Ce(NO_3)_3.6H_2O$ metal salts. The new coordination complexes C1 and C2 have been identified by spectroscopic methods. The complexes were characterized by X-ray crystallography. The nature of metal-ligand interactions was studied theoretically using NBO and EDA-NOCV analyses. The results showed that the contribution of electrostatic interactions in both complexes is considerably larger than orbital. However, the contribution of orbital interactions in $[CeL_3]^{2-}$, is more than that in $[GdL_3]^{3-}$ (28.8% vs. 21.8%). In following, the cytotoxic effect of synthetic complexes was investigated in vitro using oxaliplatin as a standard against three cancer cell lines including human breast cancer (MCF7), human colon adenocarcinoma (HT29), and human lymphocyte (HL60). The most significant inhibition activity was observed by both C1 (IC50=80.7 μM, Viability inhibition=83.41%) and C2 (IC50=98.3 μM, Viability inhibition=77.19%) toward the MCF7 cell line.

1. Introduction

Recently, the lanthanide coordination compounds have attracted the attention of scientists due to unique chemical features related to 4f electrons as well as biological properties [1–7]. Accordingly, many complexes of them have been reported which were designed from various organic ligands especially multi-dentate ligands possessing oxygen and nitrogen donor atoms [8–10] such as pyridine-2,6-dicarboxylic acid [10–13]. The studies have shown that lanthanides complexes can bind with the biomolecular targets and cause alteration in the cellular mechanism of proliferation [14]. Also, the studies have indicated that the electrostatic interaction of the metal 4f orbitals with ligand orbitals leads to bonding between these ions with ligands [15], and the formation of diverse coordination geometries [16]. Frameworks based on lanthanide coordination complexes may form novel compounds [17]. Lanthanide complexes, depending on the size of the lanthanide ion tend to have a high coordination number [18]. In 2007, in a study by Xin et al., the Ce complex containing the pyridine ligand N-phenyl 1,2 pyridine carboxamide was synthesized and the results showed the interactions between DNA and synthesized compounds are mainly intercalative [19]. In 2016, Mishra et al., synthesized new bioactive metal complexes from the reaction of Ce salt with various ligands and showed that the complexes as an antimicrobial and antioxidant are more potent than the ligands [20] In 2017, Stouder et al., reported the synthesis and characterization of a family of Ln complexes and the interaction between gadolinium complex and DNA was investigated using circular dichroism spectroscopy [21]. In 2018, Walaa et al., tested the importance of metal ion composition in biological complexes, the Zr(IV), Ce(IV), and U(VI) piroxicam anti-inflammatory drug [22]. Moreover, there are several synthesized octahedral metal complexes that have shown the remarkable inhibition against some types of bacteria, fungi and HCT-116 [23,24]. In most cases, metal complexes have shown higher biological activity than free ligands.[23,24] Efforts to synthesize anti-cancer metal complexes are still ongoing [25,26] and cancer drugs are designed to suppress disease progression and accelerate the healing process [27]. The function of these drugs means treating a wide range of uncontrolled cell growth that interferes with the growth of healthy cells [28]. The purposes of this treatment include inhibition of cell proliferation, delivery of drugs to cancer cells, specialization of drug function, rapidity and safety in the treatment of cancer, reduction of drug side effects, etc [29]. So, the mechanism of interactions between DNA and metal complexes are studied specially. Anticancer drugs break down single-stranded (SSB) and

double-stranded (DSB) DNA or may lead to the production of useless DNA or RNA. Also, these drugs prevent the actual splitting of the original cells (mitosis) of cell into two new cells. Stopping mitosis stops cell growth (replication) of cancer cells and may eventually stop the progression of cancer [30,31].

As mentioned above, lanthanide complexes with specific organic compounds can be an effective aid in creating new therapeutic agents and can be used for drugs for particular diseases [19–25]. These compounds can interact with DNA through non-covalent binding causing cleavage in the DNA strand. Cerium (IV) and Gadolinium (III) are non-toxic metal elements and can form stable complexes and some of its compounds exhibit promising anticancer effects because those are able to interact with base pairs of DNA by intercalating mode [1]. This study represents the synthesis and identification of new Ce(IV) and Gd(III) complexes with pyridine-2,6-dicarboxylic acid. After characterization of the compounds by different methods such as FT-IR, UV-Vis, CHN, and X-ray, the cytotoxic effects of the compounds are studied against cancer cell lines containing MCF7, HT29 and HL60. In addition, the strength and nature of bond in new synthesized complexes are studied theoretically.

2. Experimental section

2.1. Material and apparatus

2-aminopyridine, phenanthroline, Cerium nitrate hexahydrate, Gadolinium nitrate hexahydrate, pyridine 2-6 carboxylic acid, and solvents were purchased from Merck, Fluka, or Aldrich and were used without further purification for all synthetic works. Melting points were measured on an Electrothermal IA-9100 apparatus. Infrared spectra were collected on a Bruker Vector 22 FT-IR spectrometer using KBr pellets. CHN analyses were carried out using a Perkin-Elmer 2004 (II) elemental analyzer. UV–vis spectra were recorded on a JASCO V-570 spectrophotometer. Melting points were measured on an SMPI apparatus.

2.2. Syntheses

2.2.1. Synthesis of C1

An aqueous solution of pyridine-2, 6-dicarboxylic acid (0.33mmol, 54 mg) was added to the aqueous methanolic (1:1) solution of 2-aminopyridine (0.33 mmol, 31 mg). Then, the obtained

unclear solution was added to a stirring aqueous solution of $Gd(NO_3)_3.6H_2O$ (0.33 mmol, 149 mg) and refluxed (90 °C) for 4 h. The colorless crystals were obtained after 2 weeks. Yield (76%). M.p.: 340˚C decomp. Anal. Calc. for $C_{31}H_{27}GdN_7O_{14}$: C 42.37%, H 3.10%, N 11.16 % Found: C 42.25%, H 3.18%, and N 11.09 %. Selected IR bands (KBr pellet, cm^{-1}): 3150 ($\nu(NH)^+$), 1637s ($\nu(COO^-)$) 1458 and 1384 ($\nu C=C$). UV–Vis:ƛmax (DMSO, nm) 220.

2.2.2. Synthesis of C2

It was prepared using an identical method to C1, but $Ce(NO_3)_3.6H_2O$ (0.33 mmol, 143.29 mg) was used in place of $Gd(NO_3)_3.6H_2O$ and phenanthroline (0.33 mmol, 59 mg) in place of 2-aminopyridine. The Yellow crystals were obtained after 20 days. Yield (78%). M.p.: 357 °C. decomp. Anal. Calc. for $C_{45}H_{35}CeN_7O_{15}$: C, 51.28; H, 3.35; N, 9.30. Found: C, 51.19; H, 3.47; N, 9.45%. Selected IR bands (KBr pellet, cm^{-1}): 3138 ($\nu(NH)^+$), 1648s ($\nu(COO^-)$) 1435 and 1390 ($\nu C=C$). UV–Vis:ƛmax (DMSO, nm) 245.

2.3. X-ray crystallography

The X-ray measurement of single crystals of complexes C1 and C2 was carried out using a Bruker SMART APEX II diffractometer equipped with a CCD area detector at 298 K, with graphite-monochromated Mo-Ka radiation, k=0.71073 Å. All refinements were done by the full-matrix least-squares method on F2 using the SHELX-97 program and absorption corrections were performed using the SADABS program [32]. The crystal and structural refinement data for compounds are given in Table 1.

2.4. Computational Details

Geometry optimizations were carried out at the B3LYP [33-34] and M06 [35] levels with the def2-TZVP [36] triple-zeta basis set using the Gaussian 09 [37] set of programs. To initiate the calculations on complexes, the molecular structures of $[CeL_3]^{2-}$ and $[GdL_3]^{3-}$ in the solid state were fully optimized without any symmetry restrictions. Singlet and octet spin multiplicity were considered for $[CeL_3]^{2-}$ (without unpaired electron) and $[GdL_3]^{3-}$ (with 7 unpaired electrons) complexes, respectively. Vibrational frequency analysis, calculated at both levels of theory, indicates that the optimized structures are at the stationary points corresponding to local minima

without any imaginary frequency. The interaction energy (IE) between metal and ligands in both complexes were calculated using the following equations:

$$IE_{Ce^{4+}:L^{6-}_3} = E^{free}_{[CeL_3]^{2-}} - (E^{frozen}_{Ce^{4+}} + E^{frozen}_{L^{6-}_3})$$

$$IE_{Gd^{3+}:L^{6-}_3} = E^{free}_{[GdL_3]^{3-}} - (E^{frozen}_{Gd^{3+}} + E^{frozen}_{L^{6-}_3})$$

Where $E^{free}_{[CeL_3]^{2-}}$ and $E^{free}_{[GdL_3]^{3-}}$ are the energy of the optimized geometries of corresponding complexes. $E^{frozen}_{Ce^{4+}}$, $E^{frozen}_{Gd^{3+}}$ and $E^{frozen}_{L^{6-}_3}$ are the energy of Ce^{4+}, Gd^{3+} and L^{6-}_3 frozen in the optimized geometry of complexes, respectively. The interaction energies were corrected for basis set superposition error (BSSE) using the counterpoise method [38]. The NBO [39] analysis was carried out with the internal module Gaussian 09, at B3LYP/def2-TZVP level of theory. EDA-NOCV with the ADF 2013 package [40] was employed for analyzing the interactions in both complexes at B3LYP-D3/TZ2P(ZORA) level of theory.

2.5. Cell culture condition

MCF7 (a human breast cancer), HT29 (a human colon adenocarcinoma), and HL60 (a human lymphocyte) cell lines were purchased from the Pasteur Institute (Iran). Cells were grown in 25 cm^2 culture flasks using DMEM (Gibco, Germany) supplemented by 10% (v/v) FBS (fetal bovine serum) and penicillin/streptomycin (100 Uml^{-1}, 100 mg/ml) at 37 °C in a humidified atmosphere of 5% CO_2. They were sub-cultured regularly using trypsin–ethylenediaminetetraacetic acid (EDTA-PBS) solution (Ben Yakhte, Iran). For drug exposure experiments, compounds were dissolved in DMSO (below 0.5%) and diluted with the distilled water immediately before use.

2.6. In vitro cell growth inhibition assay (MTT assay)

Stock solutions of compounds were prepared in DMSO (below 0.5 %) and were diluted accordingly to concentrations 5-640 µM (by distilled water). Then 20 µL of solutions were added to each well and plates were incubated for 48 h. In the next step, 20 µL of MTT reagent was added with a concentration of 5 mg/mL. The cells were incubated at 37 °C in a CO_2 incubator for three or four hours. After the incubation period, the medium was removed and 200 µL of DMSO was added to each well to dissolve the produced formazan crystals by several pipetting up and

down. The absorbance values at 540 nm were determined using an ELISA reader (Bio-Rad, Model 680, USA). Untreated cells were run in each assay as the negative control group. Oxaliplatin was chosen as a positive reference. All experiments were performed in triplicate. IC_{50} values were determined after 48h [41–43].

2.7. Cell morphology analysis

The MCF7 cells were seeded in a six-well plate for 24 hours and then treated with the compounds at IC_{50} concentrations for 48 hours in 37 °C under 5% CO_2. The cell morphology was observed using an inverted fluorescence microscope [44].

3. Results and discussion

3.1. Synthesis and spectroscopic studies

FT-IR spectra of the complexes were studied in the region of 40–4000 cm $^{-1}$. The two complexes exhibited broadband at 3400–3200 cm^{-1} which can be attributed to m (OH) stretching vibrations of water molecules and pyridine-2,6-dicarboxylic acid. Stretching vibrations (NH) of ($dmpH^+$) are observed as strong bands at 3150 cm^{-1} for complex C1 and 3138 cm^{-1} for complex C2. Vibration frequencies at 3065−3013 and 2965−2948 cm^{-1} were ascribed to the (=C−H) aromatic and (C−H) aliphatic of the complexes. Also, in the middle range, the asymmetric and symmetric stretches of (COO^-) groups gave bands for C1 and C2 complexes with maxima at 1637, 1648 $cm^{-1,}$ and 1608, 1601 cm^{-1}, respectively. The absorption bands can be corresponding to m (C=C) and m (C−N) of ($pydc^{2-}$) anions at 1458–1383 and 1080–1276 $cm^{-1}$for C1 and 1435-1390 cm^{-1} for C2, respectively. The characteristic band of pyridine rings can be observed at 500–750 cm^{-1} regions for these compounds, are displayed in Fig. S1 [12,45].

Electronic absorption spectra of the two complexes (2×10^{-3} M) were recorded in dimethyl sulfoxide solution. The spectra show the strong absorptions at about 220 and 245 nm corresponding to $\pi\rightarrow\pi^*$ transition of the aromatic ring and also 285 and 275 nm related to $n\rightarrow\pi^*$ transition of the C=O chromophore for C1 and C2, respectively are showed in Fig. S2 [10].

3.2. X-ray diffraction studies of the compounds

A summary of crystallographic data is presented in Table 1 for the synthesized complexes. The complex C1 is crystallized in the monoclinic crystal system with the C2/c space group, it crystallizes with four molecules in the unit cell. In the frame work of the studies, the coordination polyhedron around Gd(III) atom is shown in Fig. 1. This complex consists of an anionic component $[Gd(pydc)_3]^{3-}$, Three cationic components $(2\text{-apyH})^{+}$,that one of them is irregular, one neutral component (2-apy) which is irregular, and two non-coordinated water molecules are formed. The anionic component of each unit $(pydc)^{2-}$acts as a three-dented ligand. Three groups of pyridine-2,6-dicarboxylate have been coordinated to each gadolinium ion. Therefore Gd(III) is nine coordinated in this structure. Selected bond lengths are listed in Table 2. The medium length of Gd–N bonds (18) is 2.518 Å and the medium length of Gd–O3 bonds (3) is approximately 2.437 Å. The sum of the three angles N1 (1-x, y, 1/2-z)–Gd–N1, N2–Gd–N1, and N1 (1-x, y, 1/2-z)–Gd–N2 is exactly equal to 359.99˚. This shows that the three atoms N1, N2, and N1 (1-x, y, 1/2-z) form a plane triangle with the Gd atom at its center. Also, the triangle formed by the three atoms O1, O5, and O3 is repeated on the sides of this triangle. The arrangement of the atoms around Gd is a slightly distorted tricapped triangular prism**.** The complex in the unit cell is observed in Fig. 3. Selected hydrogen bonds and their geometries in the accumulated are listed in Table 3. Existence of O–H···O, N–H···O and C–H···O between $(pydc)^{2-}$ and $(2\text{-apyH})^{+}$ ions as associated ions, and non-coordinated water molecules is another note that can be seen in this crystal structure showed in Fig. 2.

The complex C2 is crystallized in the triclinic crystal system and six molecules in the unit cell. As indicated in Fig. 4, this complex consists of Ce(IV) atoms and three $(pydc)^{2-}$ molecules Ce present themselves in the alignment of the pydc ligands, and these three ligands are related across a crystal center that each coordinates to one Ce(IV) atom through two oxygen and one nitrogen atoms in form of a tridentate ligand. Therefore, this complex has very similar 9-coordinate geometry to observed gadolinium. Carboxylate groups and NH in ligand are coordinated to Ce(IV) atoms. On the other hand, in the crystal structure, in addition to the complex, two Phenanetrolin are observed. The angles between coordinated atoms indicate that the central atom and ligand atoms are not in the same plane. Thus, a prism with three caps of nitrogen atoms is proved on it interestingly. Selected bond lengths are listed in Table 2. The Ce–N bond lengths in the chelated rings are almost equal, thus a prism with three caps of atoms is measured on the compound. Also, hydrogen bonding was generally observed in calculated

positions in the structure between carboxylate and phenanthroline fragment (N–H···O) lead to the formation with D···A distance ranging from 1.88(1) to 3.047(1) Å. Also extensive O–H···O, and C–H···O hydrogen bonding is observed in the structure. (see Fig. 5) and selected hydrogen bonds and their geometries in the accumulatedare listed in Table 3. Also, the complex in the unit cell is observed in Fig. 6. This complex with two triangle plane consist of N(3), O(9), O(11) and N(2), O(5), O(7) and O(1), Ce(1), O(3) atoms are three capped atoms. The sum of bond angles, N(2)–Ce(1)–N(3)=115.32(13), N(1)–Ce(1)–N(2)=122.50(13) and N(1)–Ce(1)–N(3)=122.18(13) equals to 360.00 which indicates that Ce(IV) is located in the center of N(1)N(2)N(3) (x,y, z-1) plane Ce(IV). Thus, the supposed geometry is slightly distorted tricapped. Bond distances [Ce–N=2.516(4)–2.540(4) and Ce–O=2.320(4)–2.410(3) Å {x, y, z}] are almost equal in this structure, and any collection of atoms containing (N1, O1, O3), (N2, O5, O7) and (N3, O9, O11) are located in planes.

3.3. Theoretical Studies

The optimized structures for $[CeL_3]^{2-}$ and $[GdL_3]^{3-}$ complexes, at B3LYP/def2-TZVP and M06/def2-TZVP levels of theory, are displayed in Figs. S3 and the experimental and computed important distances (Å) are compared in Table S1. The calculated root mean squares (RMS) for bond distances vary from 0.03−0.05 Å at both levels of theory, showing that the optimized structures are very close to the solid state structures.

The representative molecular orbitals of $[CeL_3]^{2-}$ and $[GdL_3]^{3-}$ complexes, in which the position of the localization of electron populations has been shown through the calculated electronic populations of the HOMO and LUMO with their energy, are depicted in Fig. 7 and Fig. 8, respectively. As can be seen, the HOMO, HOMO-1, and HOMO-2 orbitals of $[CeL_3]^{2-}$ and $[GdL_3]^{3-}$ are mainly localized over the L^{2-} ligands as the metal orbitals have a small contribution from the three HOMOs. The LUMOs in these complexes, in contrast with HOMOs, are completely different. All four LUMOs in $[CeL_3]^{2-}$ consist of 4f empty orbitals of Ce^{4+} (see Fig. 7) while, the corresponding LUMOs in $[GdL_3]^{3-}$ consist of π* anti-bonding orbitals on the ligands (see Fig. 8).

The calculated interaction energies (IE) between metal cation and three di-anionic ligands, for $[CeL_3]^{2-}$ and $[GdL_3]^{3-}$ are –2832.0 and –1905.3 kcal/mol, respectively, at B3LYP/def2-TZVP

level of theory (–2843.1 and –1952.3 kcal/mol, respectively, at M06/def2-TZVP level of theory). As can be seen, the interaction energy between the metal and ligands in $[CeL_3]^{2-}$ complex is considerably more than that in $[GdL_3]^{3-}$. However, the M–N and M–O bond lengths in $[CeL_3]^{2-}$ are slightly shorter than those in $[GdL_3]^{3-}$ (see Table S1). The calculated Wiberg bond indices (WBIs) for M–N and M–O bonds as well as the natural charges on atoms in both complexes are listed in Table S2. As can be seen, the calculated WBIs in $[CeL_3]^{2-}$, in agreement with bond lengths, are slightly more than those in $[GdL_3]^{3-}$. It should be noted that not only the both complexes have similar geometry but the number, position, and charge of di-anionic ligands are also the same. Thus, it seems that the origin of considerable difference in calculated interaction energy comes from the charge difference and electronic properties of metals and the nature of metal-ligand interactions. The values of the natural charge on Ce and Gd in $[CeL_3]^{2-}$ and $[GdL_3]^{3-}$ complexes, evaluated through a natural population analysis, are +1.39 and +1.45, respectively (see Table S2). Indeed, the values of charge transfer from three di-anionic ligands to the metal cations in $[CeL_3]^{2-}$ and $[GdL_3]^{3-}$ complexes are –2.61e and –1.55e, respectively. Thus, it seems that the covalent nature of metal-ligand interaction in $[CeL_3]^{2-}$ is more than that in $[GdL_3]^{3-}$.

To get a closer insight into the nature of the interactions between the metal and ligands in $[CeL_3]^{2-}$ and $[GdL_3]^{3-}$ complexes, EDA-NOCV [40] has been carried out at the B3LYP-D3/TZ2P(ZORA) level of theory. The interaction energy between the fragments (ΔE_{int}) in EDA-NOCV is divided into four physically meaningful components: Pauli repulsion (ΔE_{Pauli}), orbital (ΔE_{orb}), and electrostatic (ΔE_{elstat}) and, when a dispersion-corrected functional is employed, dispersion (ΔE_{disp}) is also included. So, the interaction energy is decomposed into the above-mentioned components according to the following equation:

$$\Delta E_{int} = \Delta E_{Pauli} + \Delta E_{elstat} + \Delta E_{int} + \Delta E_{disp}$$

The results of the energy decomposition analysis between the defined fragments (between metal cation and three di-anionic ligands) in the studied complexes are listed in Table 4. As can be seen, the value of the calculated ΔE_{int} in $[CeL_3]^{2-}$complex, similar to calculated IE, is considerably more than that in $[GdL_3]^{3-}$. However, the main goal of this calculation is to provide the energy components in EDA. Interestingly, the contribution of electrostatic interactions in both complexes is considerably larger than orbital interactions. The contribution of electrostatic

interactions in $[CeL_3]^{2-}$ and $[GdL_3]^{3-}$ are 71.1% and 78.0%, while the contribution of orbital interactions are 28.8% and 21.8%, respectively (see Table 4). On the other hand, the contribution of orbital interactions in $[CeL_3]^{2-}$, in agreement with the NBO results, is more than that in $[GdL_3]^{3-}$ (28.8% vs. 21.8%). As can be seen in Table 4, the contribution of dispersion forces (ΔE_{dis}) in both complexes is negligible (0.1–0.2%) in comparison with the contribution of electrostatic and orbital interactions.

3.4. Cytotoxic properties

The anti-proliferative property of the compounds was studiedusing the MTT assay against three cancer cell lines including MCF7, HT29, and HL60. The data were interpreted by cell viability curves and IC_{50} values (see Fig. 9) [46]. Both C1 (IC_{50}=80.7μM, Viability inhibition=83.41%) and C2 (IC_{50}=98.3μM, Viability inhibition=77.19%) indicated remarkable cytotoxicity against MCF7 cells specially at high concentrations. Also, potent cytotoxic effect indicated by C2 (IC_{50}=173.2μM, Viability inhibition=70.61%) compared to oxaliplatin standard drug (IC_{50}=346.9μM, Viability inhibition=53.61%) on HL60 cells while C1 (IC_{50}=653.8μM, Viability inhibition=48.61%) did not represent promising results toward mentioned cells. In a similar study, our group tested the cytotoxicity of Ce(IV) complex containing pyridine-2,6-dicarboxylate against several cancer lines and it was realized that mentioned complex has the strongest inhibitory effect toward HL60 cells (IC_{50}=100μM, Viability inhibition=52.71%) [43]. Here, the moderate inhibition effect was observed for C1 (IC_{50}=412.2μM, Viability inhibition= 54.23%) compared to oxaliplatin (IC_{50}=463.4μM, Viability inhibition=39.12%) toward HT29 cells but the cell viability curves confirmed that effectiveness of C2 (IC_{50}=178.8μM, Viability inhibition=64.39%) is relatively more potent on these cells. Generally, both complexes were effective on cell proliferation in a dose-dependent manner. Here, apoptosis as a possible pathway can suggest the death of the cells. In our previous study, cytotoxicity of pyridine-2,6-dicarboxylic acid and 2-aminopyridine evaluated on mentioned cells, and weak sensitivity was indicated by cells toward these compounds. Also, in this study, phenanthroline did not exhibit potent cytotoxicity against any of the cells tested. Organic ligands did not exhibit significant cytotoxicity toward any cancer cells tested in this study. Strong cytotoxicity by both C1 and C2 toward MCF7 cell line is a prominent property that merits these complexes to further studies in

the field of anticancer properties. Such features may be arising to the effectiveness of these compounds on disproportionate H_2O_2 and generate active intermediates [47,48].

3.5. MCF7 cells morphology analysis

Since MCF7 cells exhibited more potent sensitivity toward both synthetic complexes, these cells were selected to study morphological changes. As can be seen in Fig. 10 the cellular morphology and population in control cells are completely different from MCF7 cells treated with C1 and C2. At IC_{50} concentrations of compounds, treated cells decrease their population compared to control, and also, they became spherical and transparent. Fig. 10 (a and b) indicate that many cells have been destroyed and some completely lost their morphology. The results of this study show that these compounds probably have potent permeability ability and therapeutic effect on MCF7 cells so that they can be considered assuitable candidates in pharmaceutical fields [49].

Conclusion

The synthesis and characterization of Gd(III) and Ce(IV) complexes with pyridine-2,6-dicarboxylic acid were reported. X-ray crystallographic studies of the complexes revealed distorted tricapped trigonal prism for complexes C1 and C2. The results of theoretical studies on complexes showed that the interaction energy between the metal and ligands in $[CeL_3]^{2-}$ is considerably more than that in $[GdL_3]^{3-}$ due to the charge difference and electronic properties of metals as well as the nature of metal-ligand interactions. The contribution of electrostatic interactions in both complexes is considerably larger than orbital. However, the contribution of orbital interactions in $[CeL_3]^{2-}$, is more than that in $[GdL_3]^{3-}$. Also, MTT assays showed that C1 complex has stronger cytotoxicity than C2 against three cancer cell lines containing MCF7, HT29 and HL60.

References

[1] H. Adibi, S. Abdolmaleki, N. Shahabadi, A. Golabi, M. Mahdavi, S. Zendehcheshm, M. Ghadermazi, M. Ansari, H. Amiri Rudbari, G. Bruno, A. Nemati. Polyhedron 163 (2019) 20–32.

[2] R.C. Evans, P. Douglas, C.J. Winscom. Coord. Chem. Rev. 250 (2006) 2093–2126.

[3] M. Bottrill, L. Kwok, N.J. Long. Chem. Soc. Rev. 35 (2006) 557–571.

[4] J.C. Bunzli, G.Acc. Chem. Res. 39 (2006) 53–61.

[5] R. Darius Teo, J.S. Termini, H.B. Gray. J. Med. Chem. 59 (2016) 6012–6024.

[6] Q. Chao, X.L. Wang, E.B. Wang, Z.M. Su. Inorg. Chem. 44 (2005) 1190–1192.

[7] J.A. Peters, K. Djanashvili, C.F. Geraldes, C. Platas-Iglesias. Coordination Chemistry Reviews. Coord. Chem. Rev. 406 (2020) 213146.

[8] N.C. Martinez-Gomez, H.N. Vu, E. Skovran. Inorg. Chem. 13 (2016), 55, 10083–10089.

[9] P. Di Bernardo, P.L. Zanonato, A. Bismondo, A. Melchior, M. Tolazzi. Dalton Trans. 21 (2009) 4236–4244.

[10] D.K. Dutta, P. Chutia, B.J. Sarmah, B.J. Borah, B. Deb, J. Derek Woollins. J. Mol. Catal. A Chem. 300 (2009) 29–35.

[11] K. Butsch, A. Sandleben, M. Heydari Dokoohaki, A.R. Zolghadr, A. Klein. Inorganics. 7 (2019) 53.

[12] S. Abdolmaleki, M. Ghadermazi, M. Ashengroph, A. Saffari, S. Moradi Sabzkohi, Inorganica Chim. Acta. 480 (2018) 70–82.

[13] A. Hassanpoor, M. Mirzaei, H. Eshtiagh-Hosseini, A. Majcher. CrystEngComm. 26 (2018) 3711–3721.

[14] M. Gielen, E.R.T. Tiekink, John Wiley & Sons Ltd. Chichester, UK. 2005.

[15] W.W. Lukens, M. Speldrich, P. Yang, T.J. Duignan, J. Autschbach, P. Kögerler, Dalton Trans. 45 (2016) 11508–11521.

[16] S. Kirschener, Y.K. Wei, D. Francis, J. Berjman. J. Med. Chem. 9 (1966) 369–370.

[17] J. Robert, Hill, D.L. Long, P. Hubberstey, M. Schroder, Neil R. Champness. J. Solid State Chem. 178 (2005) 2414–2419.

[18] J. Park, J. Young Koo, H. Cheul Choi. CrystEngComm. 21 (2019) 36–41.

[19] D.J. Barnes, R.L. Chapman, R.S. Vagg, E.C. Watton. Spectrochim. Acta A. 68 (2007) 184–190.

[20] N. Mishra, K. Poonia, S.K. Soni, D. Kumar. Polyhedron 120 (2016) 60–68.

[21] E. Caitlyn, J. Stouder Khairi, F. Warren Olivia, L. Perdue Amanda, W. Stewart Clifford, J. Padgett Allison. Inorganica Chim. Acta. 464 (2017) 172–181.

[22] W.H. El-Shwiniy, W.A. Zordok. Spectrochim. Acta A. 199 (2018) 290–300.

[23] B.M. Zeglis, V.C. Pierre, J.K. Barton. Chem. Commun. 28 (2007) 4565–4579.

[24] E. Meggers, Curr. Opin. Chem. Biol. 11 (2007) 287–292.

[25] M.T. Kaczmarek, M. Zabiszak, M. Nowak, R. Jastrzab. Coord. Chem. Rev. 370 (2018) 42–54.

[26] R.D. Teo, J. Termini, H.B. Gray. J. Med. Chem. 59 (2016) 6012−6024.

[27] B. Sprangers, G. Sandhu, M.H. Rosner, P. Tesarova, W. M.Stadler, J. Malyszko. Cancer Treat Rev. 93 (2021) 102139.

[28] D. Pathania, M. Millard, N. Neamati. Adv. Drug Deliv. Rev. 61 (2009) 1250–1275.

[29] J.A. Finbloom, F. Sousa, M.M. Stevens, T.A. Desai. Adv. Drug Deliv. Rev. 167 (2020), 89–108.

[30] R. Jastrząb, M. Nowak, M. Skrobańska, A.Tolińska, M. Zabiszak, M. Gabryel, Ł. Marciniak, M.T. Kaczmarek. Coord. Chem. Rev. 382 (2019) 145–159.

[31] Y.A. Bergamo, P.J. Dyson, G. Sava. Coord. Chem. Rev. 360 (2018) 17–33.

[32] Bruker AXS Inc., SMART (Version 5.060) and SAINT (Version 6.02), Madison, Wisconsin, USA (1999).

[33] C. Lee, W. Yang, R.G. Parr. Phys. Rev. B. 37 (1988) 785–789.

[34] A.D.J. Becke. J. Chem. Phys. 98 (1993) 5648–5652.

[35] Y. Zhao, D. G. Truhlar. Theor Chem Acc. 120 (2006) 215–241.

[36] F. Weigend, R. Ahlrichs. Phys. Chem. Chem. Phys. 7 (2005) 3297–3305.

[37] M.J. Frisch, G.W. Trucks, H.B. Schlegel, G.E. Scuseria, M.A. Robb, J.R. Cheeseman, G. Scalmani, V. Barone, B. Mennucci, G.A. Petersson, H. Nakatsuji, M. Caricato, X. Li, H.P. Hratchian, A.F. Izmaylov, J. Bloino, G. Zheng, J.L. Sonnenberg, M. Hada, M. Ehara, K. Toyota, R. Fukuda, J. Hasegawa, M. Ishida, T. Nakajima, Y. Honda, O. Kitao, H. Nakai, T. Vreven, J.A. Montgomery, Jr., J. E. Peralta, F. Ogliaro, M. Bearpark, J. J. Heyd, E. Brothers, K. N. Kudin, V. N. Staroverov, R. Kobayashi, J. Normand, K. Raghavachari, A. Rendell, J.C. Burant, S.S. Iyengar, J. Tomasi, M. Cossi, N. Rega, J. M. Millam, M. Klene, J.E. Knox, J.B. Cross, V. Bakken, C. Adamo, J. Jaramillo, R. Gomperts, R.E. Stratmann, O. Yazyev, A.J. Austin, R. Cammi, C. Pomelli, J.W. Ochterski, R.L. Martin, K. Morokuma, V.G. Zakrzewski, G.A. Voth, P. Salvador, J.J. Dannenberg, S. Dapprich, A.D. Daniels, O. Farkas, J.B. Foresman, J.V. Ortiz, J. Cioslowski and D. J. Fox. Inc., Wallingford CT., 2009. 37 A. P. Scott

[38] S.F. Boys, F. Bernardi. Mol. Phys. 19 (1970) 553–566.

[39] E.D. Gladdening, A.E. Reed, J.A. Carpenter, F. Weinhold, NBO Version 3.1, 1998.

[40] G. Frenking, F.M. Bickelhaupt. in The Chemical Bond: Fundamental Aspects of Chemical Bonding, ed. G. Frenking and S. Shaik, Wiley-VCH Verlag GmbH & Co. KGaA, Chapter 4. (2014) 121−158.

[41] A. Aliabadi, E. Motieiyan, F. Hosseinabadi, M. Ghadermazi, S. Abdolmaleki. J. Mol. Struct. 1226 (2021) 129405.

[42] S. Abdolmaleki, M. Ghadermazi, F. Bagheri, H. A. Rudbari, G. Bruno, Polyhedron 176 (2020) 114292.

[43] H. Adibi, S. Abdolmaleki, N. Shahabadi, A. Golabi, M. Mahdavi, S. Zendehcheshm, M. Ghadermazi, M, Ansari, H.A. Rudbari, G. Bruno, A. Nemati. Polyhedron 163 (2019) 20–32.

[44] P. Yu, J. Deng, J. Cai, Z. Zhang, J. Zhang, M. Hamid Khan, H. Liang, F. Yang. Metallomics. 11 (2019) 1372–1386.

[45] S. Abdolmaleki, M. Ghadermazi, Inorg. Chim. Acta. 461 (2017) 221–232.

[46] S. Abdolmaleki, N. Yarmohammadi, H. Adibi, M. Ghadermazi, M. Ashengroph, H.A. Rudbari, G. Bruno. Polyhedron 159 (2019) 239–250.

[47] A. Aliabadi, M. Hakimi, F. Hosseinabadi, E. Motieiyan, V.H. Rodrigues, M. Ghadermazi, D. Marabello, S. Abdolmaleki. J. Mol. Struct. 1223 (2021) 129005.

[48] R. Heydari, E. Motieiyan, A. Aliabadi, S. Abdolmaleki, M. Ghadermazi, N. Yarmohammadi. Polyhedron 181 (2017) 114477.

[49] R. Heydari, E. Motieiyan, S. Abdolmaleki, A. Aliabadi, M. Ghadermazi, F. Bagheri, H. Amiri Rudbari. J. Coord. Chem. 73 (2020) 2347–2362.

Table 1 Crystallographic and structural refinement data for C1 and C2.

	C1	C2
Empirical formula	$C_{31}H_{27}GdN_7O_{14}$	$C_{45}H_{35}CeN_7O_{15}$
Formula weight	878.85	1069.26
Temperature/ K	293(2)	100
Wavelength/ Å	0.71073	0.71073
Crystal system	Monoclinic	Triclinic
Space group	C2/c , Z=4	P -1 (2) , Z=6
Unit cell dimensions	a = 22.0981 (4)Å b = 15.2177 (3)Å c = 16.2709 (4)Å α = 90.00˚ β = 132.166 (1)˚ γ = 90.00˚	a = 13.4254(10))Å b =20.4450(15)Å c = 23.1355(17)Å α = 81.594(2)° β = 89.012(2)° γ = 78.163(2)°
Absorption coefficient/	1.70mm^{-1}	1.20 mm^{-1}
Min. and max. transmission factor	0.721-1.000	0.659, 0.841
F(000)	2156	3239
Theta max	31.68	27.100
Index ranges	-32≤ h ≤32, -22≤ k ≤22, -23≤ l ≤23	-17≤ h ≤17,-26≤ k ≤26,-29≤ l ≤29
Crystal size (mm)	0.06 × 0.02 × 0.02	0.38 × 0.33 × 0.15
Reflections collected	64876	65558
Absorpotion corrected	Multi-scan *SADABS*	Numerical *APEX2* (Bruker, 2005)
Refinement method	Full-matrix least-squares on F^2	Full-matrix least-squares on F^2
Data /parameters	6573 / 257	27026 /1862
Goodness-of-fit on F^2	1.083	1.01
Final R indices [I>2sigma(I)]	R1 = 0.0320, wR2 = 0.082	R1 =0.055, wR2 = 0.117
R indices	wR2 = 0.0816	wR2 = 1.01
Largest diff. peak and hole	1.661 and -0.948e.Å^{-3}	5.74 and −4.22Å^{-3}

Table 2 Selected bond lengths (Å) and angles (˚) for C1 and C2.[a]

C1		**C2**	
Bond lengths		*Bond lengths*	
Gd1–O3i	2.4346 (17)	Ce1–O5	2.316 (4)
Gd1–O3	2.4346 (17)	Ce1–O1	2.320 (4)
Gd1–O1	2.4362 (16)	Ce1–O3	2.337 (4)
Gd1–O1i	2.4363 (16)	Ce1–O9	2.339 (4)
Gd1–O5i	2.4403 (19)	Ce–O7	2.377 (4)
Gd1–O5	2.4403 (19)	Ce1–N1	2.404 (3)
Gd1–N1	2.512 (2)	Ce1–N3	2.524 (4)
Gd1–N1i	2.512 (2)	Ce1–N2	2.532 (4)
Gd1–N2	2.530 (3)	*Angles*	
Angles		O5–Ce1–O1	2.540 (4)
O3i–Gd–O1	80.05 (6)	O5–Ce1–O11	78.13 (13)
O3i–Gd–O5i	78.75 (6)	O1–Ce1–O1	147.74 (13)
O3–Gd–O5i	148.21 (7)	O5–Ce1–O3	83.99 (13)
O3–Gd–O5	78.75 (6)	O1–Ce1–O3	127.43 (13)
O3–Gd–O1	80.05 (6)	O11–Ce1–O3	81.88 (13)
O1–Gd–O5	89.24 (6)	O5–Ce1–O9	76.93 (13)
N1–Gd–N1i	117.99 (9)	O1–Ce1–O9	82.38 (13)
N1–Gd–N2	121.00 (4)	O11–Ce1–O9	127.17 (13)
N1i–Gd–N2	121.00 (4)	N1–Ce–N2	122.55 (14)
O1–Gd–O5	89.24 (60	N1–Ce–N2	114.00 (14)
		N3–Ce–N2	123.45 (14)

[a] Symmetry codes: C1: (i) −x+1, y, -z+1/2, and C2 -(i) x,y, z-1.

Table 3 Selected hydrogen bonds and their geometries in the accumulated structure for C1-and C2.[a]

C1				
D–H···A	D–H	H···A	D···A	D–H···A
N3–H3A···O5^{i}	0.87 (4)	2.05 (4)	2.902 (3)	164 (4)
N3–H3B···O4^{ii}	0.81 (4)	1.99 (4)	2.808 (3)	179 (40
N4–H4···O2	0.97 (3)	1.73 (3)	2.690 (3)	168 (4)
O7–H7A···O1	0.869 (17)	2.312 (16)	3.133 (4)	158 (4)
O7–H7B···O4^{iii}	0.872 (18)	2.05 (4)	2.787 (4)	141 (5)
C13– H13···O1	0.93	2.53	3.258 (5)	135
C2				
D–H···A	D–H	H···A	D···A	D–H···A
N2H–H2HB···O8	0.8800	1.8700	2.717 (7)	162.00
C10E–H10F···O5^{v}	0.9500	2.3800	3.229 (7)	149.00
C2E–H2EA···O11^{ii}	0.9500	2.4100	3.260 (7)	149.00
C3E–H3EA···O2^{vii}	0.9500	2.4300	3.277 (8)	148.00
C5E–H5EA···O2^{vii}	0.9500	2.4500	3.297 (7)	147.00
C2F–H2FA···O4^{ii}	0.9500	2.5100	3.079(7)	118.00
C3F–H3FA···O4^{ii}	0.9500	2.3800	3.019 (7)	124.00
C1G–H1GA···O6^{ii}	0.9500	2.4200	3.251 (7)	146.00

[a] Symmetry codes: C1: (i) −x+1/2, −y+1/2, −z; (ii) x−1/2, y+1/2, z; (iii) x, −y, z+1/2, and C2-(ii) −*x*+1, −*y*+1, −*z*+1; (v) −*x*, −*y*+1, (vii) *x*+1, *y*, *z*;

Table 4 The results of the energy decomposition analysis for $[CeL_3]^{2-}$ and $[GdL_3]^{3-}$ complexes, at B3LYP-D3/TZ2P(ZORA) level of theory.[a]

Complex	Fragments	ΔE_{int}	ΔE_{Pauli}	ΔE_{elstat}	ΔE_{orb}	ΔE_{dis}
$[CeL_3]^{2-}$	$Ce^{4+} : L^{6-}_3$	–2826.5	276.8	–2205.9 (71.1%)	–893.7 (28.8%)	–3.7 (0.1%)
$[GdL_3]^{3-}$	$Gd^{3+} : L^{6-}_3$	–1924.4	159.7	–1625.2 (78.0%)	–453.7 (21.8%)	–5.1 (0.2%)

[a] Energies are in kcal/mol.

[b] Interaction energies have been calculated between two fragments: Ce^{4+} and three L^{2-} in $[CeL_3]^{2-}$, and between Gd^{3+} and three L^{2-} in $[GdL_3]^{3-}$ (see computational details).

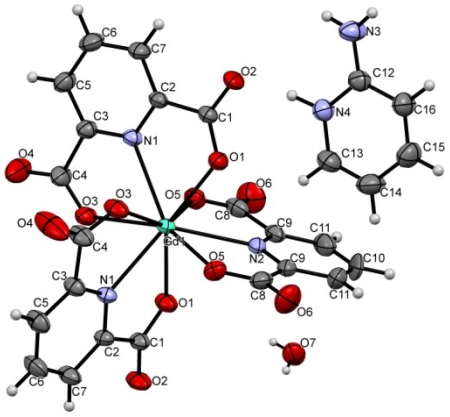

Fig. 1. Molecular structure of C1.

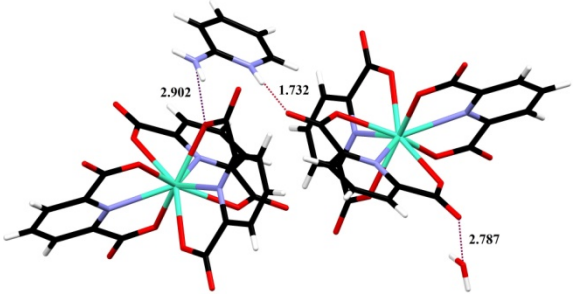

Fig. 2. Hydrogen bonds existing between complex fragments of C1.

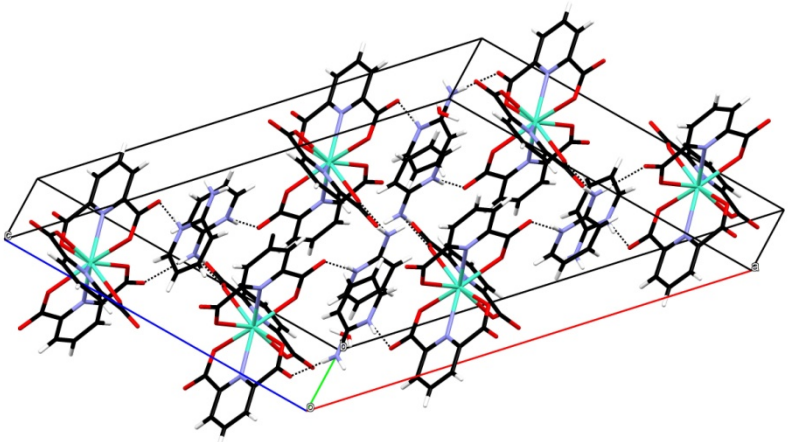

Fig. 3. Hydrogen bonds existing between layers in the unit cell of C1.

.

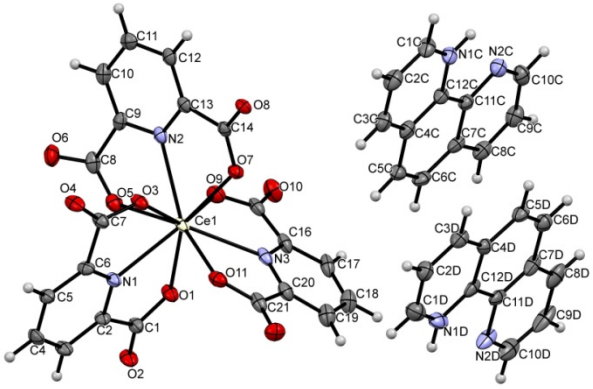

Fig. 4. Molecular structure of C2.

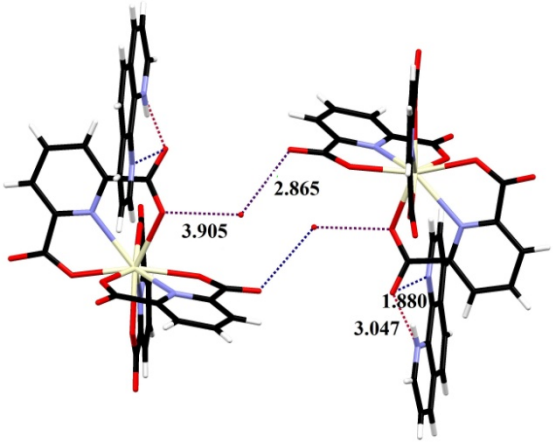

Fig. 5. Hydrogen bonds existing between carboxylate and phenanthroline fragments of C2.

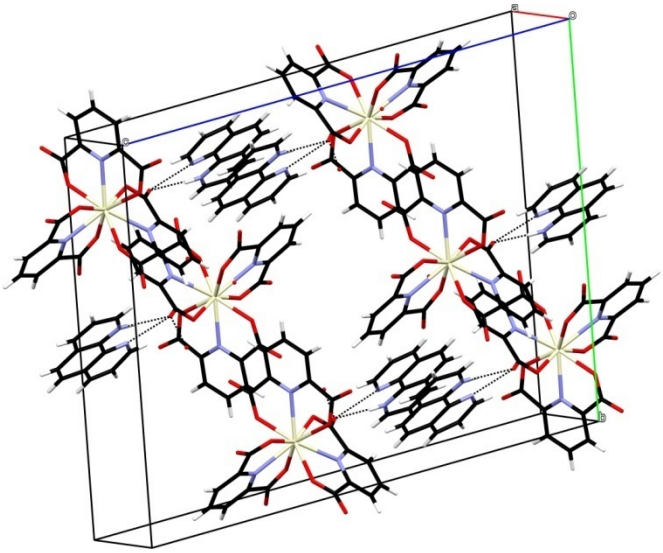

Fig. 6. Hydrogen bonds existing between layers in the unit cell of C2.

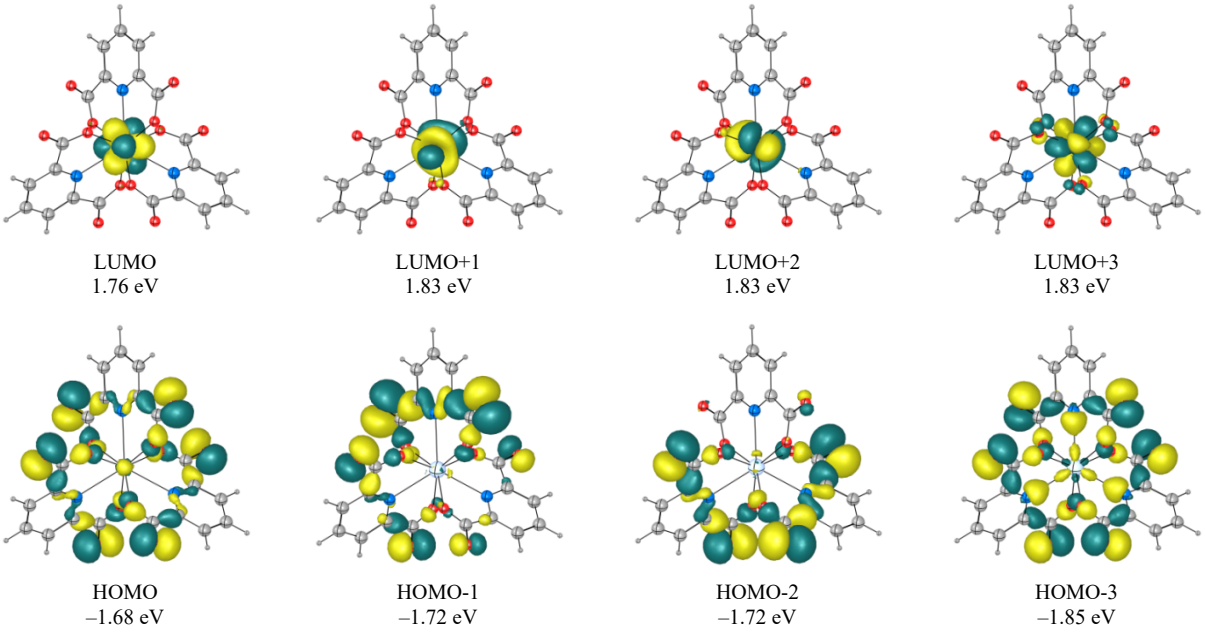

Fig. 7. Frontier molecular orbitals of $[CeL_3]^{2-}$ complex and corresponding energies (eV), at B3LYP/def2-TZVP level of theory.

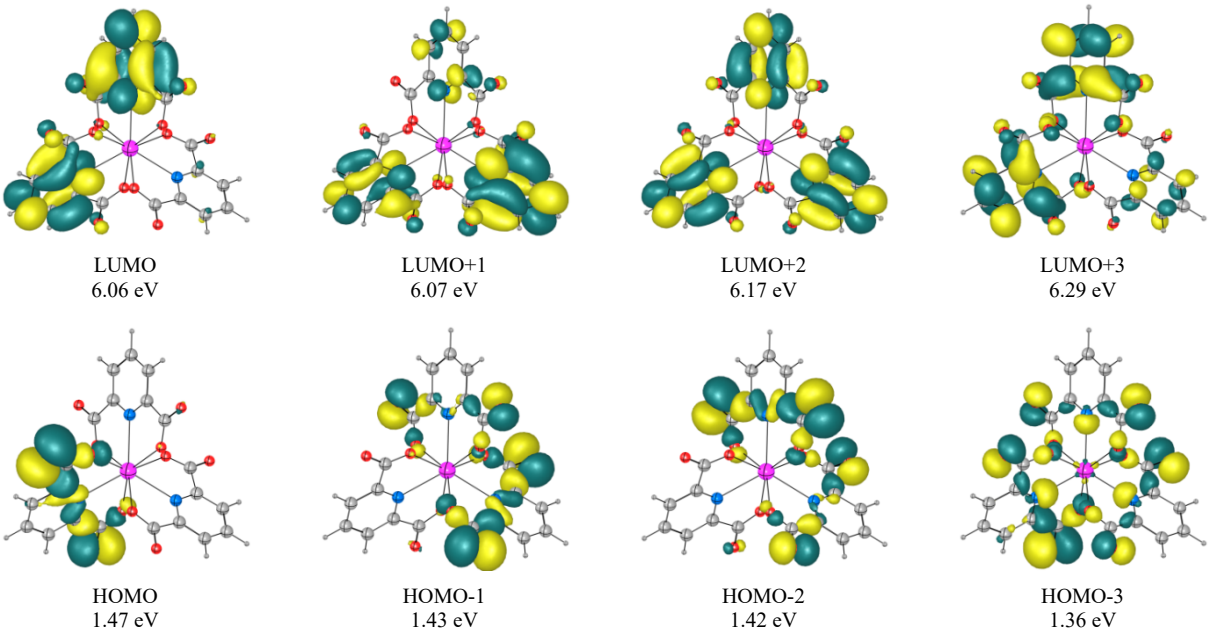

Fig. 8. Frontier molecular orbitals of $[GdL_3]^{3-}$ complex and corresponding energies (eV), at B3LYP/def2-TZVP level of theory.

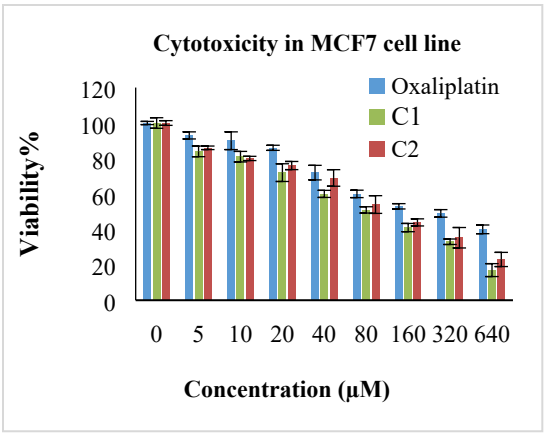

(a)

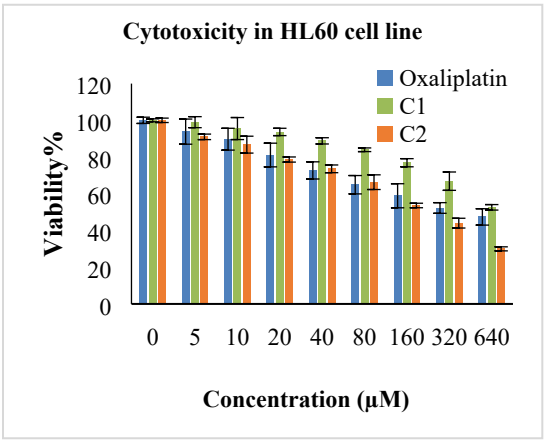

(b)

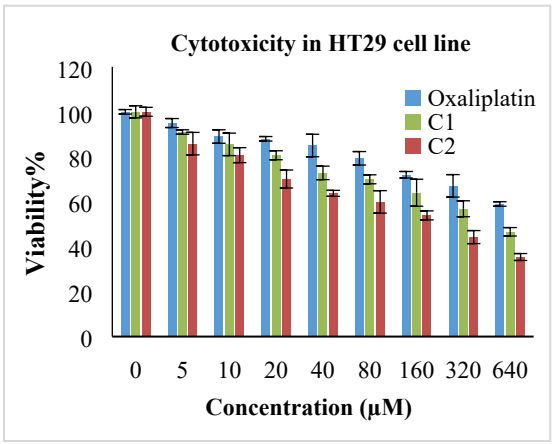

(c)

Fig. 9. Cytotoxic effect of oxaliplatin and synthetic complexes against MCF7 (a), HL60 (b) and HT29 (c) cell lines. The incubated cells were treated with concentrations 5-640µM of compounds. Cytotoxicity was determined under MTT method as explained. Data were registered as mean ±S.E.M (n=3).

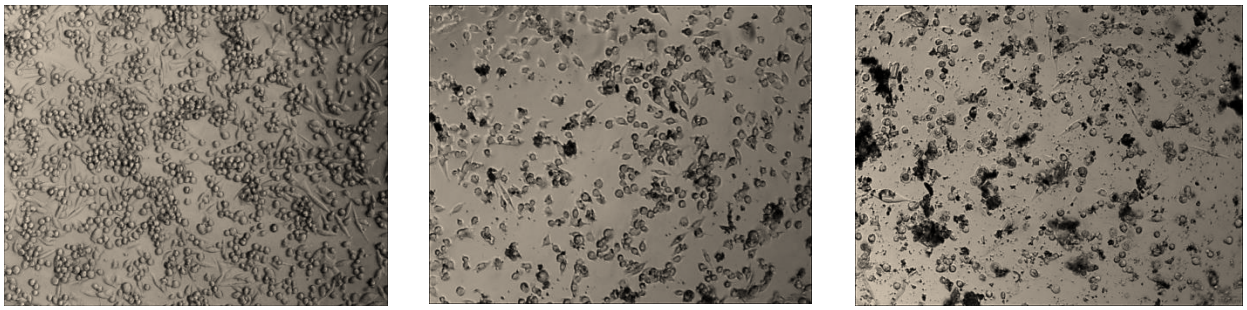

(a) (b) (c)

Fig. 10. Change in the morphology of the MCF7 cells; Control (a), Treated to C1 (80.7 μM) (b) and Treated to C2 (98.3 μM) (c), for 48 h.